IChemE

0263–8762/98/$10.00+0.00

Trans IChemE, Vol 76, Part A, January 1998

NUMERICAL MODELLING OF LIQUID WITHDRAWAL FROM GRAVURE CAVITIES IN COATING OPERATIONS

L. W. SCHWARTZ, P. MOUSSALLI*, P. CAMPBELL and R. R. ELEY*

University of Delaware, Department of Mechanical Engineering, Newark, USA
**Imperial Chemical Industries, Ltd, UK*

A numerical model is presented for the simulation of cell emptying behaviour when an engraved roller is used to transfer a liquid coating onto a moving substrate. The three-dimensional unsteady liquid motion is calculated where the flow domain is bounded above by a stress-free surface and bounded below by a moving substrate with a complex pattern of indentations. The physical model is simplified through use of the long-wave or lubrication approximation appropriate to flow in thin liquid layers. Specific predictions are made for particular cells and patterns. Cell size is found to be the principal determinant of emptying behaviour with larger cells emptying more completely. Modelling is currently restricted to the flow domain beneath the receding meniscus and drainage due to gravity. There are limitations on the dimensionless measures of coating speed. It is found that both surface tension and cell orientation are also significant in controlling the rate of drainage. Both Newtonian and shear-thinning flows are considered.

Keywords: gravure coating; mathematical modelling; time-dependent numerical simulation; lubrication theory; fluid mechanics

1. INTRODUCTION

Many industrial processes involve the application of a thin coating of a solution/suspension to a web (substrate), in order to alter the surface characteristics of the web after subsequent drying of the liquid (often water). This enables a wide range of product characteristics to be created; for example antistatic properties, better ink adhesion for printing applications, or improved adhesion of vacuum deposited metals to provide an oxygen barrier for food products, etc. Minimizing the variability of these surface characteristics is often a stringent requirement, depending on the market for the product. It is therefore important to choose a coating process capable of applying the liquid to the specified level of uniformity. A wide range of coating operations utilize roll coating technologies to apply the liquid film to the moving web. Many different methods of application exist ranging from single to multiple roll systems. In some cases, the main factor controlling the thickness of the film is determined by the flow characteristics between a pair of rolls; primarily the roll velocities and the gap between them. Alternatively, a gravured/knurled roller may be used, so called due to the large number of cells (typically 10s to 100s of microns in size) engraved throughout its surface. These cells retain liquid when the roll is removed from a bath or enclosed chamber of coating fluid; a proportion of this liquid is then given up to a rubber applicator roll (e.g. offset coating) or straight onto the web (direct gravure coating).

The advantage of using a gravured roll is that the coating thickness and its variability, especially in the transverse direction, is to a large extent governed by the volume (and variability in volume) of the cells which are engraved into the roll's surface. As the engraving process can be carried out very accurately, this enables the coat weight range to be chosen, and a high degree of uniformity to be achieved. In order to specify the design of a gravure roll, a method is needed to predict the fraction of liquid which is removed from the cells. As experimental time on production lines becomes ever more costly, there is a growing advantage in being able to predict these figures from theory. Therefore, a program of work was initiated at the University of Delaware to model the process of liquid evacuation from cells, as a function of cell size and shape, with the objective of identifying the critical parameters needed to optimize the design, with respect to cell evacuation fraction. This paper summarizes the findings to date from this study. Both two-dimensional and three-dimensional simulations have been carried out and are described.

In the following section approximate evolution equations are presented for flow beneath a receding meniscus and also for gravity-driven flow down a vertical substrate. For both problems the substrate contains gravure indentations. Each of these two problems correspond to a local solution for a portion of the flow on an engraved roller, as shown on the schematic diagram in Figure 1.

There does not appear to be previous work on three-dimensional simulation of thin layer flows over engraved surfaces. Kim *et al.*[1] treat thin-layer flows over roughened surfaces, as related to spin coating. They assume an axisymmetry geometry and treat the roughness as statistical. The authors have previously considered quasi-static motion over regular patterns of differing wettability[2,3], which is analogous to a doubly-periodic undulating surface. In that work however, the goal was to explain the phenomenon known as 'contact-angle hysteresis,' wherein the location of

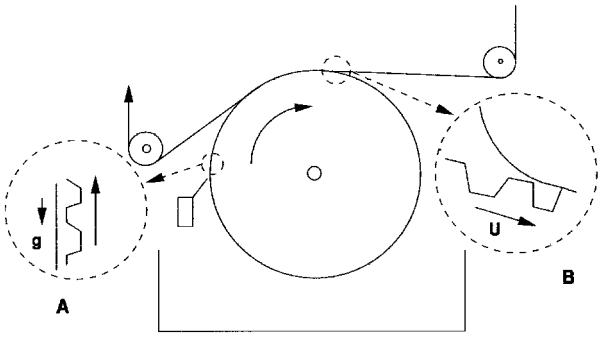

Figure 1. Schematic diagrams of direct gravure coating. The rotating gravure wheel lifts the liquid coating out of a bath and deposits it onto a moving web. The two problems treated here are gravity-driven drainage from the cells above the metering knife (inset A) and withdrawal from beneath a pinned meniscus where the gravure wheel leaves the web (inset B).

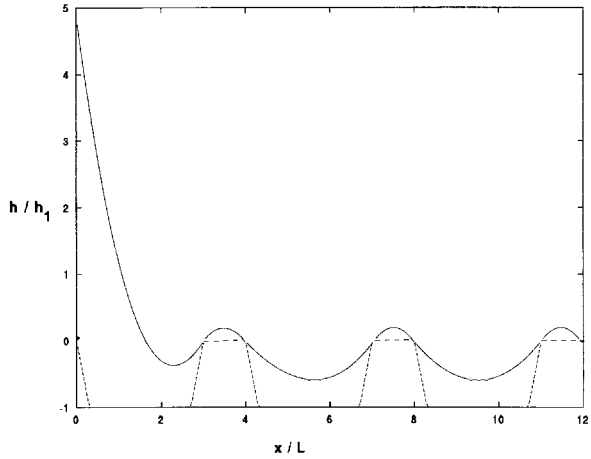

Figure 2. A frame from a two-dimensional time-dependent simulation. The indented gravure plate is moving from left to right. The ordinate and slope of the liquid surface (meniscus) are specified at the left boundary. In this and the following two figures, the vertical scale is in units of the cell depth while the horizontal scale is in units of the characteristic length L from equation (3a). See text for other parameter values.

a macroscopically observable contact line, where a liquid, vapour, and dry solid meet, depends on whether the liquid is advancing onto, or receding from, the dry surface. The liquid motion was assumed to be so slow that viscous forces could be neglected; the free surface of the liquid proceeds from one local minimum-energy equilibrium configuration to another where only body forces and surface tension are considered. Because of the limitation to very slow motions, the work is not applicable to the present problem; it does, however, indicate the importance of representing the full two-dimensional surface description of the substrate. It was found that actual contact line motions differ greatly from motions on surfaces whose properties change in one direction only.

Benkreira and Patel[4] did experimental work using a laboratory-scale direct roll coating apparatus. They used three different gravure cell patterns and found significant differences in cell emptying among the three, which they attributed primarily to cell-size effects.

In the following section, a mathematical model leading to evolution equations for the liquid layer thickness variation will be developed. Finite difference methods for solving the equations are given in section 3. Some calculated unsteady flows are shown in section 4.

2. THE MATHEMATICAL MODEL

2a. Two-Dimensional Unsteady Flow

Before proceeding to the flow model in three space dimensions, a simpler two-dimensional model will be presented. A Newtonian liquid layer is considered bounded above by a tractionless free boundary upon which surface tension acts: $z = h(x, t)$ is the equation of the free boundary relative to the nominally flat or 'land' area of the engraved plate. Thus h is measured from the zero level of the vertical scale in Figure 2. The layer is bounded below by a rigid substrate that is moving to the right with constant speed U. Let $h_1(x, t)$ be the equation of the substrate; it satisfies the equation

$$h_{1t} = -Uh_{1x} \tag{1a}$$

where the x, t subscripts signify partial derivatives. This equation states that, in a fixed coordinate system, the moving gravure is a constant waveform that is moving from left to right with speed U. The total layer thickness $h_2 = h - h_1$ satisfies the lubrication evolution equation

$$h_{2t} = -Q_{2x} = -\left[Uh_2 + \left(\frac{\sigma}{3\mu}\right)h_2^3 h_{xxx}\right]_x. \tag{1b}$$

Here Q is areal flow rate. Adding equations (1a) and (1b) gives the final evolution equation for the surface,

$$h_t = -\left[Uh + \left(\frac{\sigma}{3\mu}\right)(h - h_1)^3 h_{xxx}\right]_x. \tag{2}$$

An equation equivalent to (2) has been used by Kim *et al.*[1] for a stationary rippled substrate. $h_1(x, t)$ is the supplied function for substrate shape, satisfying equation (1a); in general $h_1 \leq 0$.

All dimensional constants in equation (2) can be absorbed by the following scaling. Let h_0 be a measure of coating thickness, such as the gravure cell depth, to which h and h_1 are referenced. x is made dimensionless using the substrate length scale

$$\bar{L} = \bar{h}_0\left(\frac{\sigma}{3\mu U}\right)^{1/3} \tag{3a}$$

and the time unit

$$T^* = \frac{L}{U}. \tag{3b}$$

With the scalings (3a,b), the evolution equation, using dimensionless variables, is simply

$$h_t = -\left[h + (h - h_1)^3 h_{xxx}\right]_x. \tag{4}$$

The trapezoidal teeth or cells on the moving plate in Figure 2 are conveniently generated by

$$\xi = x - t \tag{5a}$$

$$\eta = \xi - a\,\mathrm{Int}\left(\frac{\xi}{a}\right) \tag{5b}$$

$$H = \mathrm{Min}\left[\eta/b, (w - \eta)/b, d\right] \tag{5c}$$

$$h_1 = -\mathrm{Max}(0, H) \tag{5d}$$

Here 'Int' signifies the 'integer part function', i.e. the largest integer not greater than the argument. Equations (5) generate a moving substrate of wavelength a with gravure widths w, as measured at the level of the top of the teeth, wall slope $1/b$, and depth d. Without loss of generality, we set $d = h_0$; thus the gravure depth is one in dimensionless units.

Initial and boundary conditions also need to be supplied. At the downstream or right end of the computational window, $x = x_1$ say, we use the simple conditions

$$h_x(x_1) = h_{xxx}(x_1) = 0. \tag{6a, b}$$

Because the coating thickness h at the right exit $x = x_1$ is not specified, the total throughput will arise as part of the solution. In particular, it is controlled primarily by variations in the upstream meniscus curvature. At the upstream or left end, nominally $x = 0$, we fix the value of h and the slope h_x,

$$h(0) = h^*, \tag{6c}$$

$$h_x(0) = h_x^* - \tan(\pi - \hat{\theta}_a). \tag{6d}$$

For definiteness h^* maybe identified as the distance between the 'web' and the gravure land level. In scaled units, $\hat{\theta}_a$ may be thought of as the 'advancing contact angle' for the liquid moving onto the dry web, that, notionally, is moving from right to left, as the gravure moves from left to right. Before entering the computational window, from the left, the gravure is fully flooded. Using equation (3a), the unscaled 'advancing contact angle' θ_a is given by

$$\tan(\pi - \theta_a) = \left(\frac{3\mu U}{\sigma}\right)^{1/3} \tan(\pi - \hat{\theta}_a).$$

An alternative explanation for the boundary conditions (6c,d) can be given when the gravure plate and the web are widely separated at the receding meniscus. Far away from the gravure plate, viscous forces are small and the meniscus curvature can be assumed to be constant. By fixing both the altitude h^* and slope h_x^* at the same point, one can, in effect, specify the meniscus curvature, which, in turn, is determined by the nip location. This curvature is, within the thin-layer small-slope approximation, given by

$$\kappa = \frac{h_x^{*2}}{2h^*}. \tag{7}$$

Justification for the use of constant-curvature meniscii when the altitude h is large can be found in the asymptotic analyses of Landau and Levich[5] and Bretherton[6].

Our primary interest is 'steady-state,' i.e. time-periodic, motion and the resulting dependence of residual cell liquid volume on input parameter values; thus the initial condition required to start the computation is less important, in the present context. For definiteness a decaying exponential is chosen for $h(x, 0)$ satisfying the boundary condition (6c).

2b. Three-Dimensional Unsteady Flow

Consider a substrate pattern of indenture in two dimensions (x, y) where x is taken in the direction of motion. Ellis-model shear-thinning rheology is also included. According to this model[7], the viscosity μ is assumed to depend on the stress stress τ,

$$\frac{1}{\mu} = \frac{1}{\mu_0}\left(1 + \left|\frac{\tau}{\tau_{1/2}}\right|^{\alpha-1}\right). \tag{8}$$

Here the input parameter $\tau_{1/2}$ is the value of shear stress at which the viscosity is equal to one-half the low-stress Newtonian value μ_0. The degree of shear-thinning is also controlled by the input exponent α; $\alpha = 1$ corresponds to Newtonian flow and $\alpha < 1$ is the range for shear-thinning behaviour. The Ellis model is a typical generalized-Newtonian flow law; other laws, for particular applications, can be implemented without difficulty.

If z is the distance measured normal to the substrate and the no-slip condition is applied on the substrate and the condition $\tau = 0$ on $z = h$, the constitutive law $\tau = \mu u_z$ can be integrated to find the velocity profile across the thin liquid layer. The integral of the velocity is the vector flux $\mathbf{Q}$ which, in dimensional variables, is given by

$$\mathbf{Q} = -\frac{\nabla p}{3\mu_0}(h - h_1)^3 \times \left[1 + \left(\frac{3}{\alpha + 2}\right)\left(\frac{|\nabla p|(h - h_1)}{\tau_{1/2}}\right)^{\alpha-1}\right] + Uh\mathbf{i} \tag{9}$$

where U is the substrate speed in the positive x direction and $\mathbf{i}$ is a unit vector. Here the pressure gradient has contributions from capillary pressure and gravity which is assumed to be aligned with the substrate in the positive x direction. Thus

$$\nabla p = -\sigma\nabla\nabla^2 h + \rho g\mathbf{i}.$$

The evolution equation for the free surface follows from application of the global mass conservation equation

$$h_t = -\nabla \cdot \mathbf{Q}, \tag{10}$$

where ∇ is the two-dimensional differential operator with respect to the orthogonal substrate coordinates x and y. A gravity drainage lubrication flow in one space dimension, using the Ellis model, is discussed in Reference 8.

Two special cases will be considered. These are (i) withdrawal of the gravured substrate from beneath a pinned meniscus as in section 2 above, and (ii) gravity drainage from a vertical section of the gravure lying above the knife blade and corresponding to inset (A) in Figure 1.

For the first problem, the two-dimensional model above generalizes to

$$\frac{\partial h}{\partial t} = -\frac{\partial h}{\partial x} - \nabla \cdot (s\nabla\nabla^2 h) \tag{11}$$

using the substrate length and time scales previously given in equations (3). Calculated results will only be shown for Newtonian liquids; thus the permeability is simply $s = (h - h_1)^3$.

The second problem is gravitational drainage on a gravure pattern. Here the Ellis model will be retained but substrate motion will be ignored. This problem will be used to assess the importance of non-Newtonian effects and also the effect of cell orientation. The relevant dimensionless evolution equation is

$$\frac{\partial h}{\partial t} = -\frac{\partial s}{\partial x} - \nabla \cdot (s\nabla\nabla^2 h), \tag{12}$$

and s includes the factor in square brackets in equation (9). For this problem, the substrate length unit is

$$L_1 = \left(\frac{\sigma h_0}{\rho g}\right)^{1/3}, \tag{13a}$$

and the unit of time is

$$T_1^* = \frac{3\mu_0 L_1}{\rho g h_0^2}. \tag{13b}$$

Several three-dimensional cell patterns have been investigated. Typically, cell walls consist of intersecting planes. The cells used in the following examples have flat bottoms and tapered side walls and are generated by a two-dimensional generalization of the Minimax procedure given in equation (5) above. The family of cells are trapezoidal solids, essentially similar to the pattern termed 'quadrangular' by Benkreira and Patel[4]. This cell is used either with straight sides parallel to the flow direction or turned 45° to the flow. Still more complicated cell shapes may be produced by repeated application of the above Minimax method. A representative gravure pattern is shown in Figure 3.

3. NUMERICAL IMPLEMENTATION

The dimensionless form of equations (11) and (12) is solved by a finite difference method in space and time. The substrate is discretized into an $M \times N$ rectangular computational domain. Spatial derivatives are approximated using central differences; thus the method is second-order accurate in space. For the results presented below, symmetry boundary conditions were imposed on three of the four sides, i.e.

$$h_n = h_{nnn} = 0 \tag{14}$$

where n is distance in the normal direction at each boundary. Time marching is made efficient using a novel semi-implicit method. It is similar, in principle, to alternating direction (ADI) methods used for second-order diffusive problems, as discussed by Peaceman[9]. Nonlinear pre-factors in s are evaluated at the 'old' time level. Thus the method is only first-order accurate in time. However convergence is easily verified under temporal refinement and time-steps are adjusted accordingly. Because of the severe stability requirements for an explicit solution, i.e.

$$\Delta t < O(\Delta x)^4,$$

the present method is faster by several orders of magnitude compared to an explicit scheme. It is also much faster than time integration were the ADI not used, in which case very large banded systems of equations would have to be solved. Further details of the numerical algorithm, as applied to coating flows on smooth substrates, have appeared[10].

For a given simulation, computer usage is proportional to the number MN of calculated h values. Typical calculations require a few minutes on a PC with a Pentium Pro 200 processor, using the UNIX operating system. Surface profiles are displayed dynamically during the calculation and can be saved for further use either electronically or on videotape.

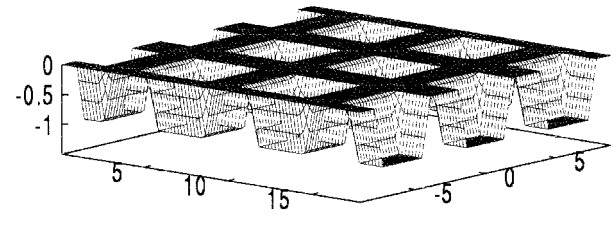

Figure 3. A periodic square array of gravure cells. The cell pattern moves to the right at unit speed. The same pattern is used in all calculations shown here; only the period or wavelength is varied.

4. CALCULATED RESULTS AND DISCUSSION

A periodic array of cells is first considered, arranged in a square pattern and equation (11) solved corresponding to the receding meniscus at inset B of Figure 1. The computational window used is three cells long and wide as shown in Figure 3. Each individual cell is trapezoidal in shape. The land area between adjacent cells has a width equal to one-half the cell width at the top or land level. The cell area, on the land, is thus 44 per cent of the total land area. The entire pattern moves to the right as the computation proceeds. Three different cell sizes are used, differing in size by a factor of four between the largest and smallest. While the dimensionless variables used allow families of shapes to be analysed at once, and the physical parameter values only enter the problem via the units of substrate length and time in equations (3), it is useful to identify a representative set of physical parameters corresponding to industrial coating conditions. Using viscosity $\mu = 0.05$ poise, $\sigma = 70$ dynes cm^{-1} and $U = 200$ cm sec$^{-1} = 400$ ft min^{-1}, the capillary number is $Ca = \mu U/\sigma = 0.14$. Taking the cell depth equal to 20 μm gives a character length $L = 26.7$ μm. The pattern wavelength for the 'medium' cells is 160 μm, while the 'small' cells have a spacing of 80 μm and the spacing for the 'big' cells is 320 μm. For comparison, 200 lines-per-inch patterns have a wavelength of about 120 μm. Thus, with the above choice of physical parameters, patterns investigated fall within the domain of interest. Also of importance, in assessing the validity of these results, is the Reynolds number $Re = (\rho U h_0)/\mu$. Using the above physical values, $Re = 8$, suggesting that inertial effects, not considered here, may modify the results somewhat. Strict satisfaction of the condition that Re be small requires coating speeds substantially less than the 400 ft min^{-1} value suggested above.

In each of the simulation results presented here, the free surface is pinned at $(x, h^*) = (0, 5)$. Unless stated otherwise, the slope there $h_x^* = -5$ in dimensionless units. Starting with an initial exponential shape, the liquid surface variation becomes time-periodic after passage of about three cells. The computational window is fixed in space while the gravure pattern moves at constant speed in the direction of x increasing. The 'steady-state' motion becomes periodic with a period equal to the cell passage time, the time required for any given cell to move one wavelength downstream.

Figure 4 is a snapshot of the liquid surface, above the cells, for the medium cell case, with cell wavelength W equal to $6L$, after the motion has become periodic. The x and y scales are in units of L. The manner in which the meniscus 'scrapes out' the cells can be seen in this figure. Similar snapshots for the small and large cell cases, $W = 3L$ and $12L$ respectively, show less and more indented surfaces above the cells corresponding to less and more fractional removal of the original liquid content of the cells. Note that, because the liquid surface must be continuous, and the model assumes perfect wetting of the gravure material, the land area in each of these figures is not dry. A small, but not

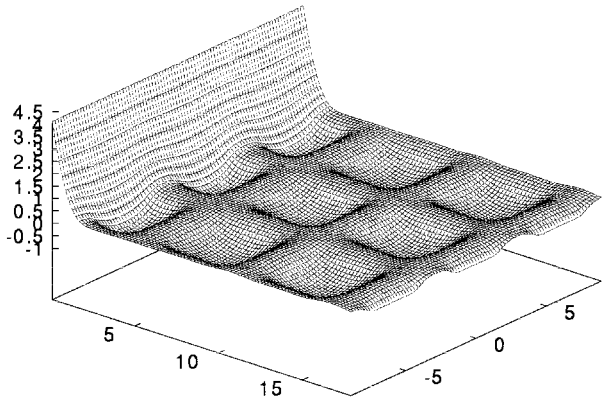

Figure 4. The liquid surface for the medium-sized cell for meniscus withdrawal. Using physical values in the text, the period is 160 μm. $t/T^* = 48$. Full-established pattern. Note how the meniscus 'scrapes out' the cells.

insignificant, fraction of the liquid carried away by the gravure is on the lands, rather than in the cells.

Quantitative information for the degree of cell emptying is given in Figure 5. The liquid/fraction is plotted within the cells versus time for the small, medium, and large-cell cases. The plot shows these quantities averaged over all cells within the computational window. A fraction of the cells lie under the meniscus at any time and the cells under the meniscus are full. This fraction varies with time with a period equal to the cell passage time. Thus the plot consistently overpredicts the cell liquid fraction remaining, but the curve minima, within the periodic range, should give a close estimate of the final liquid fraction in a given cell. For the big cells this fraction is about 0.48 increasing to 0.92 for the small cells. Also shown for comparison is a curve labelled 'medium grooves'. These are cells whose width is equal to that of the medium cells, but each 'cell' extends completely across the moving plate. The resulting flow is, by symmetry, entirely in the x-direction and is identical to the two-dimensional cases treated in section 2. The groove case was included to show the important of dimensionality.

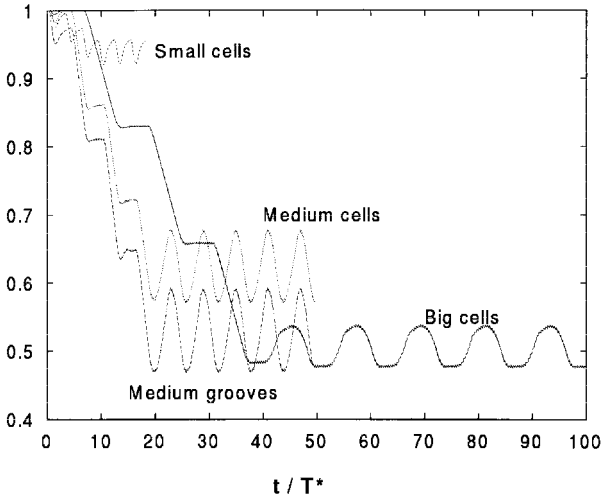

Figure 5. Average liquid fraction in cells versus time. Three cell sizes are compared. The ultimate period in each case is the cell passage time. The medium cell pattern can be compared with the medium grooves, a two-dimensional flow field.

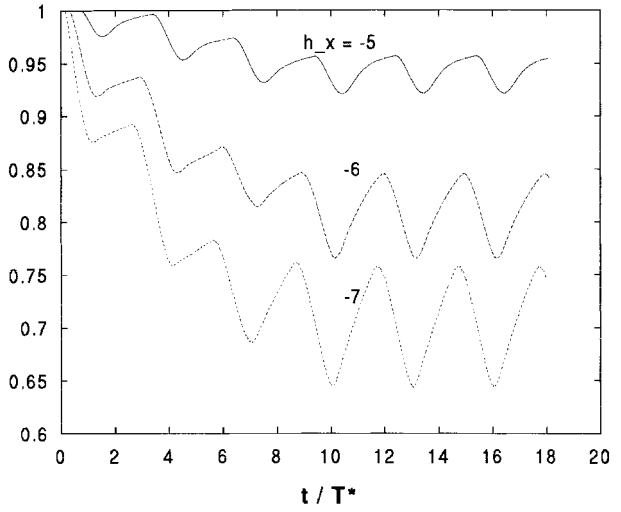

Figure 6. Average liquid fraction in the small cell pattern versus time, for three values of the imposed meniscus slope shown. The curvature of the meniscus, away from the gravure is proportional to the square of the slope.

The medium grooves has a residual fraction of about 0.47 compared with 0.58 for the medium cells.

Figure 6 provides similar information, using the small cell pattern, and shows the effect of meniscus curvature. According to equation (7), at a given fixed value of h^*, which is large compared to the coating layer thickness, the curvature κ is proportional to the square of the slope there. Keeping the surface ordinate constant at the left boundary of the computational domain, but varying the slope there, allows the meniscus curvature effect to be ascertained. For the three values of slope shown on the figure, encompassing about a factor of two in meniscus curvature, the residual fraction varies between 0.92 for the loosely curved meniscus to 0.64 for the tightly curved case.

For the gravity drainage problem, results are presented for a single cell on an otherwise flat substrate. Representative cells are of various widths W, all with the same quadrangular shape, i.e. a truncated four-sided pyramid. The flat area at the bottom of each cell has a width equal to $0.3W$. Results are given for two values of the initial land-area coating thickness, $0.1h_0$ and $0.05h_0$, and for two cell orientations, sides aligned with the body force, termed 'square' and 'rotated 45°, termed 'diamond.' The computational domain is a 60×60 mesh, though only half this number needs to be computed because of assumed bilateral symmetry. The gravure cell is 20 mesh units wide. Initially the free surface is taken to be uniform except for two rows at the upstream end where the coating thickness is very small in order to restrict inflow.

In general, when gravity drainage is the only mechanism for cell emptying, realistically small cells as used in gravure coating retain virtually all their content for long times. For example, with the physical parameters $\rho = 1$ gm cm^{-3}, $g = 980$ cm sec^{-2}, $\sigma = 40$ dyne cm^{-1}, $\mu = 0.05$ poise and cell depth $h_0 = 40$ μm, the characteristic length $L_1 = 580$ μm and $T_1 = 0.35$ sec.

Figure 7 is a late-time picture of the free surface for a large $W = 10L_1$ cell in the diamond orientation with respect to the direction of gravity. Gravity causes flow from left to right in the figure. The gravure cell shape is superimposed and its tapered shape can be seen. The remaining liquid

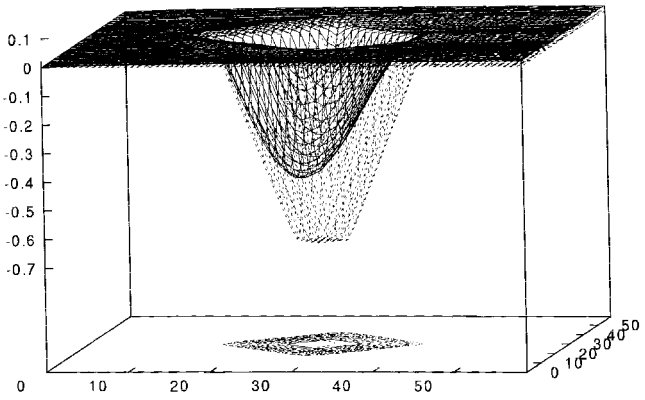

Figure 7. Late time picture of free surface superimposed on large diamond-shaped gravure cell in gravity drainage. The cell width $W = 10L_1$. The cell depth is 70 per cent of the initially-uniform coating film thickness at the start of the simulation. The residual liquid volume is 33%.

volume, equal to 33 per cent of the initial volume, is seen to be nonuniformly distributed. More liquid is 'piled up' near the downhill end of the cell. Such large cells empty quickly with the bulk of liquid emerging as a single coherent drop. Compared to the square orientation, the diamond cell empties more readily because of a tendency, in the case of the diamond, for the liquid to run down the cell edges to the downstream 'point' where the resulting concentrated mound more easily escapes the retarding effect of surface tension. In the square orientation, calculations suggest that an irreducible liquid volume may remain as time becomes infinite. The sharp edges of the cell cause the free surface above these edges to become highly curved. The liquid pressure at these edges, because of surface tension, becomes large and drives fluid away. The liquid coating thickness there quickly thins, becoming, thereby, effectively impermeable and preventing further drainage from the cell. Such behaviour, for coating films on substrates with regions of large curvature, has previously been reported[11].

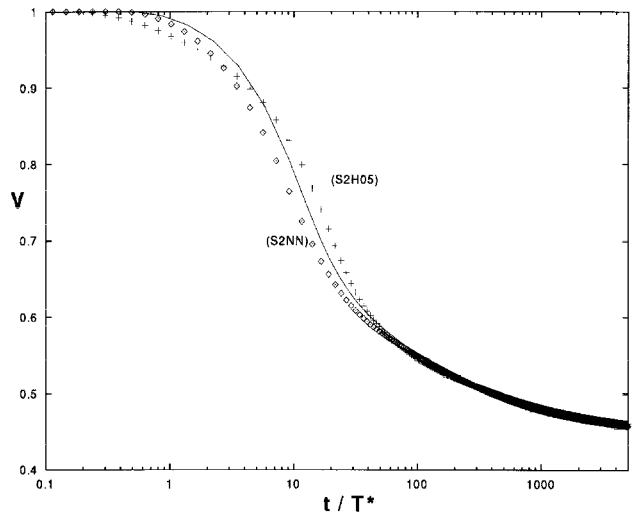

Figure 8. Remaining liquid volume fraction versus dimensionless time for gravity drainage for a square cell of width $2L_1$. Solid line and symbols (S2H05) are for Newtonian liquids with different initial land coating thicknesses. S2NN is a shear thinning liquid with $\alpha = 1.5$.

Figure 8 gives drainage histories and includes two additional effects: initial land coating thickness and non-Newtonian behaviour. For all three curves in the figure the square orientation is used and the cell size is $W = 2L_1$. The solid curve has an initial land coating height equal to $0.1h_0$ while the crosses are for an initial land coating of $0.05h_0$. The liquid is Newtonian for both these cases. The diamond symbols, labelled (S2NN), uses a liquid that is shear-thinning with an Ellis exponent α, in equation (9), equal to 1.5. Thus, at high rates, this liquid has a viscosity that decreases as the reciprocal square root of the shear stress. The constant $\tau_{1/2}$ is chosen so that a uniform layer of thickness $0.1\,h_0$ has the same viscosity as the Newtonian liquid. At early times, the viscosity of the shear thinning liquid within the cell is about half as great as the Newtonian value, due primarily to the greater depth and consequent higher stress there. The cell empties a bit more quickly, initially. Ultimately, the drainage becomes limited by the formation of almost dry regions near the sharp edges, as explained above, and the long-time emptying is virtually the same for the three cases.

Drainage has been considered from a pattern of cells in addition to the single-cell cases shown above. For a square pattern of cells, as cells empty some of their liquid content flows into cells lying immediately below. It is possible that this effect can be minimized by skewing the cell positions with respect to the drainage direction. This effect will also be present in the meniscus withdrawal problem and cell emptying may be improved for suitable skewed cell patterns.

5. CONCLUSIONS

A mathematical model has been developed to describe two important effects relevant to cell emptying in direct gravure roll coating. These are the time-periodic motion when an engraved plate moves under a partially-constrained liquid meniscus and the free drainage from gravure cells on a stationary or moving vertical plate due to gravity. The theory used is a simplification of the governing equations, appropriate to flow in thin layers where the dominant forces result from surface tension, gravity, and viscosity. Compared to the exact theory for flow of Newtonian liquids, the simplified theory is valid when certain dimensionless parameters are sufficiently small. These parameters are the capillary number $Ca = (\mu U)/\sigma$, Reynolds number $Re = (\rho U h_0)/\mu$, and appropriate measures of the free-surface and substrate slopes. Extended lubrication analyses have been performed in simple problems to find the higher-order correction in capillary number[6] and the leading-order effect of finite Reynolds number[12]. *Ca* corrections are expected to be small but *Re* effects require further investigation. Experiments[4] show some *Re* dependence on coating film thickness. An alternating-direction implicit scheme provides efficient time-dependent simulation of the model. The basic result of the present work is that increasing the size of the gravure cells will greatly increase the degree of cell emptying.

Because the starting slope or meniscus curvature is an input parameter, the model is currently incomplete. A fully predictive model of the gravure coating process will include a unified treatment of the flooded region between the roller and the web as well as the meniscus withdrawal region treated here. Studies of the flooded region

in two-dimensional problems are available and employ either lubrication theory[13] or finite-element analysis[14]. Such a unified model must also account for the effects of web tension, speed, and wrap angle, the latter referring to the angular extent of the region where the gravure roller and web are in close contact, as shown in Figure 1. The present pinned meniscus removes the possibility of the so-called ribbing instability which is often observed in high-speed roll coating applications as a transverse oscillation of this meniscus[14].

The present simulation assumes that thin liquid films are stable on the gravure material; i.e. there is no tendency to de-wet. This corresponds to a static contact angle, for the coating liquid on the gravure material, that is close to zero. In this case it is predicted that the land area will retain a non-negligible amount of coating liquid. It is possible that this liquid fraction has been previously considered to be resident in the gravure cavities, thus overestimating the cell fraction remaining there. Wetting behaviour on both the gravure roller and the web will also be affected if surfactant is present in the liquid coating. Surface tension gradient effects may become important and can be included in the mathematical model[15].

Three-dimensional effects lead to a significant increase in the predicted residual liquid fractions compared to two-dimensional grooves of the same shape. This could have been anticipated since the liquid surface, above a partially-filled gravure cell, is 'supported' in all four sides by the cell side walls in three dimensions. Cell orientation, equivalent to rotating the square cell pattern 45° into the diamond position appears to improve emptying behaviour. The present procedure can be used to investigate a variety of periodic patterns in order to optimize performance.

REFERENCES

1. Kim, J. S., Kim, S. and Ma, F., 1993, *J Appl Phys*, 73: 422–428.
2. Schwartz, L. W. and Garoff, S., 1985, *Langmuir* 1: 219–230.
3. Schwartz, L. W. and Garoff, S., 1985, *J Colloid Interf Sci*, 11: 422–437.
4. Benkreira, H. and Patel, R., 1993, *Chem Eng Sci*, 48: 2329–2335.
5. Levich, V., 1962, *Physicochemical Hydrodynamics*, (Prentice-Hall, Englewood Cliffs).
6. Bretherton, F., 1977, *J Fluid Mech*, 10: 166.
7. Bird, R. B., Armstrong, R. C. and Hassager, O., 1977, *Dynamics of Polymeric Liquids*, (Wiley, New York).
8. Weidner, D. E. and Schwartz, L. W., 1994, *Physics of Fluids*, 6: 3535–3538.
9. Peaceman, D., 1977, *Fundamentals of Numerical Reservoir Simulation*, (Elsevier, Amsterdam).
10. Weidner, D. E., Schwartz, L. W. and Eres, M. H., 1997, *J Colloid Interf Sci*, 187: 243–258.
11. Schwartz, L. W. and Weidner, D. E., 1995, *J Engineering Maths*, 29: 91–103.
12. Chang, H.-C., 1994, *Ann Rev Fluid Mech*, 26: 103–136.
13. Savage, M. D., 1982, *J Fluid Mech*, 28: 443–455.
14. Coyle, D. J., Macosko, C. W. and Scriven, L. E., 1986, *J Fluid Mech*, 171: 183–207.
15. Schwartz, L. W., Cairncross, R. A. and Weidner, D. E., 1996, *Physics of Fluids*, 8: 1693–1695.

ACKNOWLEDGEMENT

This work is supported by ICI, The State of Delaware, and the NASA Microgravity Program.

ADDRESS

Correspondence concerning this paper should be addressed to Professor L. W. Schwartz, Department of Mechanical Engineering, University of Delaware, Newark, DE 19716, USA.

The manuscript was received 6 October 1997 and accepted for publication after revision 10 December 1997.